Front Propagation in Patterned Precipitation. 3. Composition Variations in Two-Precipitate Stratum Dynamics

Maysam Msharrafieh, Mazen Al-Ghoul, Hazar Batlouni, and Rabih Sultan*

Department of Chemistry, American University of Beirut, P.O. Box 11-0236, 1107 2020 Riad El Solh, Beirut, Lebanon

Received: January 18, 2007; In Final Form: May 8, 2007

This paper is a study of the composition dynamics of Liesegang band strata of $Co(OH)_2$ and $Ni(OH)_2$ from NH_4OH, with redissolution by complex formation with ammonia. At a fixed time, the cobalt hydroxide composition was found to exhibit a random variation with band number, yet within a general overall decrease. The decrease with band number becomes more pronounced as the initial concentrations of Co^{2+} and Ni^{2+} get closer to each other. At equal concentrations, periodic oscillations in $Co(OH)_2$ composition appear over consecutive bands. The time evolution of the total $Co(OH)_2$ mass percent (over the entire pattern of strata) passes through a maximum. The dynamics of this complex system has been simulated by theoretical calculations using the model of Müller and Polezhaev, modified by Al-Ghoul and Sultan in a series of two papers in *J. Phys. Chem. A*; the present paper is the third in the series. The simulations capture the essential features of the experimentally observed dynamics.

1. Introduction

This paper is an extension of past work on periodic preceipitation, both in experiment[1] and in theory.[1−3] Pattern formation could be defined as the appearance of an array of similar units that repeat with a certain defined or undefined symmetry.[4] One classical example of pattern formation is the display of spatial oscillations due to periodic precipitation, the so-called Liesegang banding phenomenon,[5−7] emerging from the coupling of the precipitation reaction with diffusion.[7,8] When a gel solution, containing a certain electrolyte (called the inner electrolyte), is placed in a test tube with another electrolyte (the outer electrolyte) diffusing from its top, a precipitate pattern appears as a set of bands that form parallel to the diffusion front down the tube, separated by clear, distinct spaces. Spatial oscillations are thus manifested through the alternation of precipitate and precipitate-free domains, in the form of bands or rings. The variation of the conditions under which precipitate patterns are formed reflects on the morphological structure of the pattern, as well as its dynamic properties.[9]

The precipitate bands formed may be static or locked: i.e., once formed, they maintain their position in space. Dynamic precipitate patterns (either a single band or a set of bands) are those in which diffusion and precipitation processes couple in a nonequilibrium regime to a redissolution reaction. In a vertical tube, the upper gel portion (close to the interface between the two electrolytes) is more influenced by the excess diffusing electrolyte, which causes the redissolution of the preformed precipitate bands, whereas at the bottom of the tube precipitate bands persist much longer. A gel containing Co^{2+} displays $Co(OH)_2$ bands upon diffusion of NH_4OH, used as the outer electrolyte. Later, the $Co(OH)_2$ bands near the interface redissolve, forming $Co(NH_3)_6^{2+}$ in excess NH_4Cl.[10−12] Thus, new bands are formed at the bottom, and old ones dissolve at the top, and the whole pattern appears as a set of strata migrating down the tube. There are many examples of such dynamic systems reviewed in refs 10, 11, and 13−15. The coupling of diffusion, precipitation, and redissolution governs the dynamics of such migrating Liesegang patterns. Complex formation and its effect on periodic precipitation systems by provoking the partial redissolution of the precipitate have stimulated considerable interest and have been the subjects of a number of theoretical modeling investigations.[2,3,16,17]

The introduction of a foreign cation that competes with Co^{2+} for both precipitation and complex formation could interfere with the processes involved and is thus expected to significantly alter the dynamics of the $Co(OH)_2$ system.[1] The dominance of complex formation with ammonia for the foreign ion suppresses the dissolution of cobalt hydroxide. Ni^{2+} is one such suitable foreign ion, because the solubility product constant of $Ni(OH)_2$ is similar to that of $Co(OH)_2$, while the formation constant for the $Ni(NH_3)_6^{2+}$ complex is a few orders of magnitude higher than that of $Co(NH_3)_6^{2+}$. Table 1 presents the values of the solubility product constants and the complex formation constants for both ions.

The effective reaction schemes representing the precipitation and dissolution scenario in the presence of NH_4OH are, for cobalt

$$Co^{2+}(aq) + 2NH_4OH(aq) \rightarrow 2NH_4^{+}(aq) + Co(OH)_2(s) \quad (1)$$

$$Co(OH)_2(s) + 6NH_4^{+}(aq) + 4OH^{-}(aq) \rightarrow Co(NH_3)_6^{2+}(aq) + 6H_2O(l) \quad (2)$$

and for nickel

$$Ni^{2+}(aq) + 2NH_4OH(aq) \rightarrow 2NH_4^{+}(aq) + Ni(OH)_2(s) \quad (3)$$

$$Ni(OH)_2(s) + 6NH_4^{+}(aq) + 4OH^{-}(aq) \rightarrow Ni(NH_3)_6^{2+}(aq) + 6H_2O(l) \quad (4)$$

Note that the redissolution reactions (eqs 2 and 4) differ from those that appear in refs 1−3, 9, 10, and 31 in that they are

* To whom correspondence should be addressed. E-mail: rsultan@aub.edu.lb.

10.1021/jp070423o CCC: $37.00
Published on Web 06/28/2007

TABLE 1: Solubility Products (K_{sp}) for the Hydroxides and Formation Constants (K_f) for the Ammonia Complexes of Co^{2+}, Ni^{2+}, Ca^{2+}, and Mg^{2+} [a]

ion	CN	K_{sp}	K_f
Co^{2+}	6	3.00×10^{-16}	5.00×10^{4}
Ni^{2+}	6	2.00×10^{-16}	2.00×10^{8}
Ca^{2+}	6	6.00×10^{-6}	1.99×10^{-6}
Mg^{2+}	4	1.80×10^{-11}	0.10

[a] CN = coordination number. Values were taken from refs 18 and 19.

rewritten in basic medium, thus reflecting the experimental conditions more accurately. This modification does not affect the reaction scheme adopted in the theoretical treatment of section 4.1 because it fits the simplified picture by essentially preserving the stoichiometry of the complex. Note that eqs 2 and 4 have the equilibrium constants $K = 4.4 \times 10^{17}$ and 1.7×10^{21}, respectively (K is calculated using the expression $K = K_{sp}K_f/(K_b)^6$, where K_b is the ionization constant for ammonia ($=1.8 \times 10^{-5}$) and K_{sp} and K_f are given in Table 1).

Of particular interest in the present study is the effect of the initial concentrations of Co^{2+} and Ni^{2+} (cations within the inner electrolyte in gel), as well as the outer ammonium hydroxide concentration. A higher nickel concentration gives a wider uniform precipitate zone at the top and delays the band formation. An earlier investigation of such a system showed that a sole uniform precipitate zone propagates down the tube above a cutoff of $[Ni^{2+}]_0 = 0.13$ M, when $[Co^{2+}]_0$ is 0.10 M (the subscript 0 denotes initial concentration), irrespective of the concentration of NH_4OH used.

Studies on multicomponent Liesegang systems are rather scarce in the literature. Some casual patterns have been reported,[11] and a few thorough studies have been conducted in two-[1,20−22] and three-precipitate[23] systems. We here focus on band composition in the $Co(OH)_2-Ni(OH)_2$ system and to that end have carried out a systematic quantitative analysis to determine the spatio−temporal variation of the precipitate mass proportions within the bands. Such a study has not been conducted before, as the literature overwhelmingly treats Liesegang patterns with single-salt systems, stressing the variation of the number of bands,[24] band thickness,[25] and band spacing[26,27] with electrolyte concentrations, in both time and space. The composition of the $Co(OH)_2-Ni(OH)_2$ bands over the entire span of the strata, its spatio−temporal variation, and its correlation to the initial concentrations of cations in the gel are investigated here. After an analysis of the experimental results, we present a comprehensive computational study of our system, through a full-scale solution of the kinetic equations describing the underlying dynamics. The model equations involve diffusion and chemical reaction rate laws.

2. Experimental Section

The experiments have been performed in the limit of large initial concentration difference (Δ)[10,24,28] between the interdiffusing electrolytes (outer and inner electrolytes). In a two-salt precipitate system, two factors are also worth considering: the difference in the concentrations of the inner electrolytes ($\delta = [Co^{2+}]_0 - [Ni^{2+}]_0$) and their stoichiometric ratio ($\rho = [Co^{2+}]_0/[Ni^{2+}]_0$).

The required masses of $CoCl_2 \cdot 6H_2O$ (Fluka) and $NiSO_4 \cdot 6H_2O$ (Mallinckrodt) were weighed to the nearest 0.1 mg and transferred to a beaker containing 25.00 mL of doubly distilled water, to obtain solutions with the desired concentrations.

A 1.250 g portion of gelatin (Difco) was added (to make a 5% gelatin solution), and the solutions were heated with continuous stirring until all the gelatin dissolved, at which stage the solutions started to boil. The resulting gel was immediately placed in a set of five test tubes (35 cm long with 0.4 cm diameter), each two-thirds full. The upper edge of the gel was marked to indicate the interface between the gel and the upper solution. The tubes were covered with Parafilm paper and allowed to stand for at least 12 h at room temperature. Then 13.37 M ammonium hydroxide solution was added to the remaining one-third empty portion of each tube (marking initial time $t = 0$) above the solidified $Co^{2+}-Ni^{2+}$ gel interface. The interface between the gel and the outer electrolyte was marked in all tubes. Since one tube at a time was cut for quantitative analysis, a set of tubes was prepared and monitored under exactly the same experimental conditions. As these patterns were essentially quite reproducible, we assumed that each of those five tubes represented a fixed, individual time in the evolution of the same pattern. The use of different tubes was necessary, as every tube was inevitably destroyed for band analysis, and thus the time sequence could not be perpetuated in the same tube. The minimum time for the appearance of bands was 2−3 days. The spatial variation in band composition was studied at time intervals of 5 days, and the experiment spanned a period of 25 days. At the required time to be measured, pictures of each tube were taken with a digital camera (Sony, DSC-F717) and then the tube was cut at both ends and the gel was allowed to slide out onto a glass plate using mild water pressure from a syringe connected to the medium through a short Tygon channel. The bands were labeled, individually isolated, and cut from edge to edge in regions where they were clear. In a preliminary numbering, we started from the bottom of the set of strata to its top, until the fuzzy region near the interface was reached, where no clear distinction of separate bands could be made. This was done because we did not know how far on the top we could reach, with such very closely spaced bands. Once we isolated the bands, however, the numbers were exactly reversed to reflect the realistic situation starting with band 1 at the top and ending with the last band at the bottom. All the band numbers appearing in the figures are thus consistent with that latter numbering. Each band was meticulously cut at its edges, placed in a minimum amount of 0.3 mL of 1.0 M HCl with initial stirring, and left until the whole band was dissolved. Then 2.0 mL of doubly distilled water was added to dilute the solutions of dissolved precipitates. Because of the low solubility product constants for both $Co(OH)_2$ and $Ni(OH)_2$ (Table 1), we assumed that, within a band, all the cations from the gel were precipitated as their hydroxides.

Flame atomic absorption (AA) spectrophotometry (SOLAAR Atomic Absorption, Thermo Lab Systems) was used to determine the content of cobalt and nickel in the dissolved precipitate bands. The concentrations of Co^{2+} and Ni^{2+} in the original samples were relatively high, which necessitated further dilution to a range of good detection by flame absorption. For this reason, 0.10 mL of each solution of a given dissolved band was delivered into a 10 mL volumetric flask and diluted to the mark, thus yielding a 100× diluted solution. This procedure was repeated for three sets of systems, experiment I (0.250 M Co^{2+}, 0.100 M Ni^{2+}), experiment II (0.200 M Co^{2+}, 0.150 M Ni^{2+}), and experiment III (0.175 M Co^{2+}, 0.175 M Ni^{2+}), every 5 days over a period of 25 days. The results of the analyses by atomic absorption gave the concentrations in the diluted samples of atomic cobalt and nickel in mg L^{-1}, to the nearest 0.007 mg L^{-1}. The proportions were converted to masses and mass percentages of $Co(OH)_2$ and $Ni(OH)_2$ as follows: the raw concentrations (of Co^{2+} and Ni^{2+}) from AA measurements

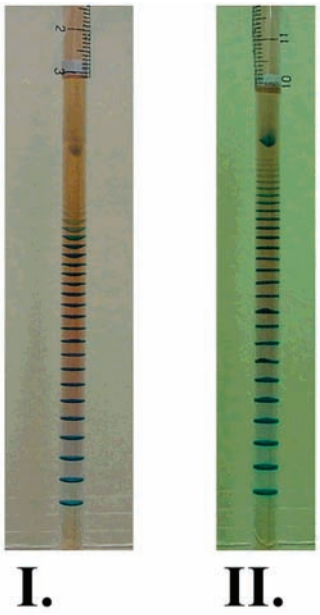

Figure 1. Liesegang patterns in tubes for experiments I and II, at time $t = 25$ days: (I) $[Co^{2+}]_0 = 0.250$ M, $[Ni^{2+}]_0 = 0.100$ M ($\delta = 0.150$ M); (II) $[Co^{2+}]_0 = 0.200$ M, $[Ni^{2+}]_0 = 0.150$ M ($\delta = 0.050$ M). In both experiments, $[NH_4OH]_0 = 13.37$ M. The redissolution of the $Co(OH)_2$ bands appears clearly at the top of the tube.

multiplied by the volume of solution (10.0 mL) yielded the masses of elemental cobalt and nickel in the 0.10 mL aliquot. To get the mass within the band, we multiplied by a factor of 2.3/0.10, where 2.3 mL is the total volume of starting solution (water + acid), in which the band was dissolved. The masses of the hydroxides were then deduced as $m_{Co(OH)_2} = M_{Co(OH)_2} \times m_{Co}/M_{Co}$, with a similar calculation for nickel (m and M denote actual mass and molar mass, respectively). The mass percent for each hydroxide was then calculated relative to the total mass. The mass balance for Co and Ni over the entire spatial span of the tube is discussed in Appendix A.

3. Results

Three comprehensive experiments were performed, each corresponding to a specific choice of δ. A picture of typical patterns at the specified time is shown in Figure 1.

3.1. Experiments at $\delta = 0.150$ and $\delta = 0.050$. *3.1.1. Experiment I.* The first experiment performed corresponds to the most widely distant initial cation concentrations: namely, 0.250 M Co^{2+} and 0.100 M Ni^{2+} ($\delta = 0.150$ M), with 13.37 M outer electrolyte. This system is a dynamic pattern, manifesting a propagation through a gradual disappearance of the continuous precipitate zone at the tail and an advancement via new band formation at the head. A picture of typical patterns at the specified time is shown in Figure 1. For the particular pattern of experiment I, the continuous precipitate zone appears before day 5, at which time the upper bands start to separate and then completely dissolve at later times, thus gradually increasing the distance of the first band from the interface. Concurrently, new precipitate bands form at the head (bottom of the tube). The illusion of pattern propagation is clearly the result of the dynamics of precipitation and redissolution. Pictures of the evolution of this pattern, taken every 5 days, are displayed in Figure 2. The bands through the whole pattern actually maintain their spatial location and do not move. However, during the pattern evolution, each band undergoes a change of its content in both precipitates: $Co(OH)_2$ and $Ni(OH)_2$.

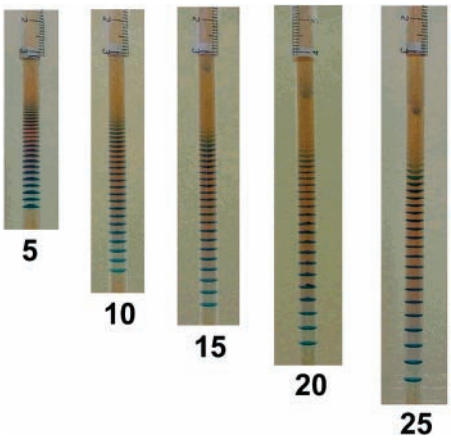

Figure 2. Time sequence for a propagating Liesegang pattern in experiment I. The time (in days) is shown under each tube.

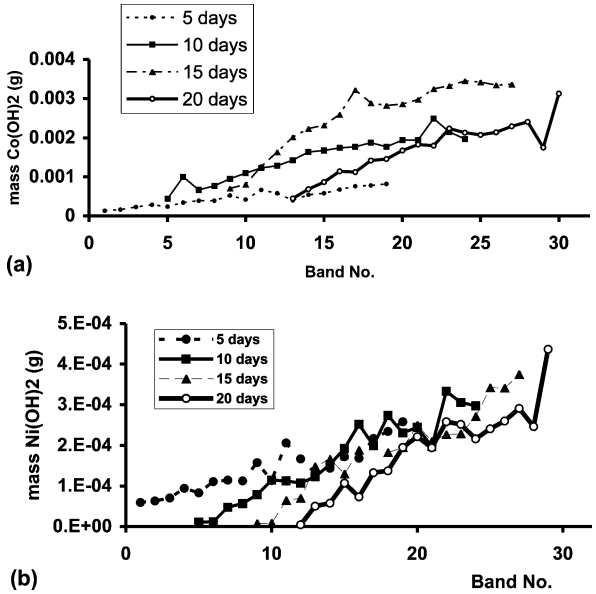

Figure 3. (a) Distribution of the mass of $Co(OH)_2$ over the bands of the pattern in experiment I, at times of 5, 10, 15, and 20 days. (b) Spatial variation of the mass of $Ni(OH)_2$ at the same times as in (a). The masses of both hydroxides gradually increase with band number.

Figure 3 shows a plot of the masses of $Co(OH)_2$ and $Ni(OH)_2$ (in grams) with band number at four selected times. A plot of percent composition by mass of $Co(OH)_2$ versus band number (obtained from the aforementioned masses), at the indicated times, is shown in Figure 4.

3.1.2. Experiment II. We then decreased the initial cobalt ion concentration and increased that of the nickel ion in the gel. The system corresponds to the following initial conditions: 0.200 M Co^{2+}, 0.150 M Ni^{2+} ($\delta = 0.050$ M), and 13.37 M outer electrolyte. The visual appearance of the time evolution of the pattern in experiment II (not displayed here) greatly resembles that in experiment I, depicted in Figure 2. The morphological characteristics of the bands in the two patterns also exhibit a good similarity, as clearly revealed in Figure 1. The mass variation of $Ni(OH)_2$ (we display the masses of one precipitate here) and with the variation of the $Co(OH)_2$ mass percent composition over the spatial sequence of band strata, at five selected times, are displayed in Figure 5.

At fixed time, within a given pattern, there is an overall increase in the masses of $Co(OH)_2$ and $Ni(OH)_2$ (Figures 3 and 5a). Three important conclusions can be deduced from the composition plots in Figures 4 and 5c. First, the dissolution of

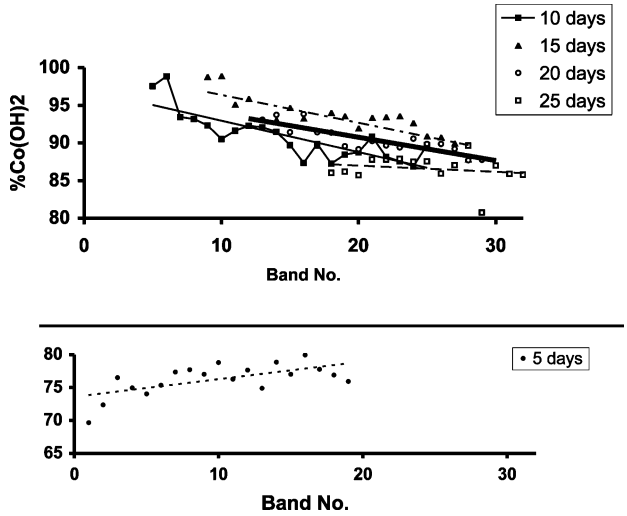

Figure 4. Variation of the mass percent composition with band number in experiment I, at times of 5, 10, 15, 20, and 25 days, with best-fit straight lines. The slopes of the lines are recorded in Table 2. The composition displays random oscillations (see the joined points at $t = 10$ days) with band number instead of a monotonic trend. Over the entire pattern at a fixed time, however, the percent composition exhibits an overall decrease.

both precipitates is more pronounced in the upper bands, where dissolution is dominant because of high ammonia concentration in this region. Second, the mass of cobalt hydroxide precipitate is dominant in the whole pattern, consistent with the initial concentrations, since the initial Co^{2+} concentration used is larger than that of Ni^{2+}. Third, the dissolution of nickel hydroxide decreases in the lower portion of the tube, in favor of a prevailing precipitation. This is clearly manifested in the decrease in the percentage of cobalt hydroxide. Therefore, complex formation and the subsequent predominant dissolution of nickel hydroxide appear to be the dominant factor in delineating the characteristics of the pattern.

The faster kinetics of cobalt hydroxide precipitation relative to that of nickel hydroxide is revealed in the last band at certain times, which has low masses in both precipitates but significantly higher composition in $Co(OH)_2$, thus causing an abrupt increase in the latter and, hence, a sharp break in the trend. The small masses are due to the fact that the band has not completed its formation. Although we expect a relatively richer $Ni(OH)_2$ content because of no significant dissolution of $Ni(OH)_2$ in that region, a sharp increase in the percentage of $Co(OH)_2$ is obtained. This clearly reveals that, at early stages of the band formation, $Co(OH)_2$ experiences a faster precipitation kinetics. Note that such points were neither shown in the plots nor obviously included in the trend calculation. Their dynamic evolution is, however, very informative.

An intriguing property of the dynamics of this system is that the variation of composition with band number is not monotonic or smooth but, rather, is characterized by random oscillations. However, within this overall erratic spatial distribution, the percentage of cobalt hydroxide generally *decreases* as we go down the tube. Generally decreasing trends are obtained for both experiments. This is once again consistent with the enhanced precipitation of nickel hydroxide in the bands remote from the interface. Therefore, dissolution by complex formation with ammonia has little effect, due to the decrease in $[NH_4^+]$ in that region. However, the overall average percentage of $Co(OH)_2$ remains greater than that of $Ni(OH)_2$ in all of the bands, due to a higher initial cobalt concentration in the gel medium.

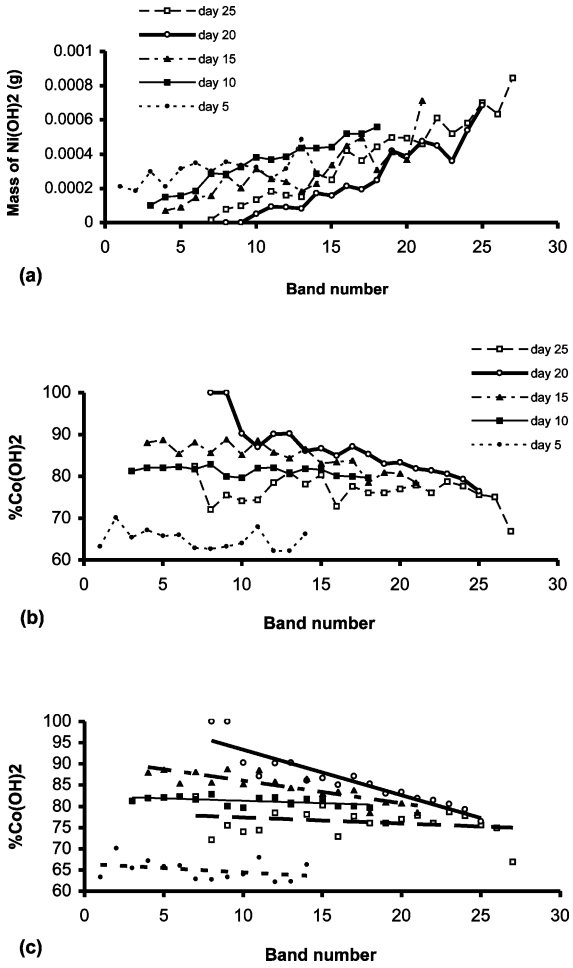

Figure 5. (a) Distribution of the mass of $Ni(OH)_2$ over the bands of the pattern in experiment II, at times of 5, 10, 15, and 20 days. The mass generally increases with band number. (b) Variation of the mass percent composition in $Co(OH)_2$ with band number at times of 5, 10, 15, 20, and 25 days. (c) Same as in (b), but with best-fit straight lines. The slopes of the lines are recorded in Table 2.

3.2. Oscillations at $\delta = 0$. *3.2.1. Experiment III.* In order to search for a correlation between the spatio−temporal evolution of these systems with initial concentration, a third set of conditions was chosen for study. The initial concentrations chosen were 0.175 M Co^{2+}, 0.175 M Ni^{2+}, and 13.37 M NH_4-OH outer electrolyte in 5% gelatin medium. Here δ (the difference in inner electrolyte concentrations) is equal to zero. We emphasize that the morphology of this pattern is not similar to that of the other two discussed before. Band splitting is observed. The propagating strata display band doublets that are very close to each other, near the interface, which at later times separate in space, as shown in Figure 6.

The split bands appear each as one doublet group, distinctly separated from other doublets. The constituent bands of each doublet group have contrasting intensities, indicating that both precipitates in each individual band have different densities. In each pair of split bands, the lower band is denser than the upper one. One could predict an alternation in the composition of the precipitates over the various strata, by merely noticing the intensity of the bands: one is distinctly darker than the other. This was indeed confirmed by the quantitative analysis of the bands, which revealed oscillations in composition over successive strata. Such oscillations in the percent composition of $Co(OH)_2$ are shown in Figure 7. This alternation is the result of the splitting of the same band into two domains of distinctly

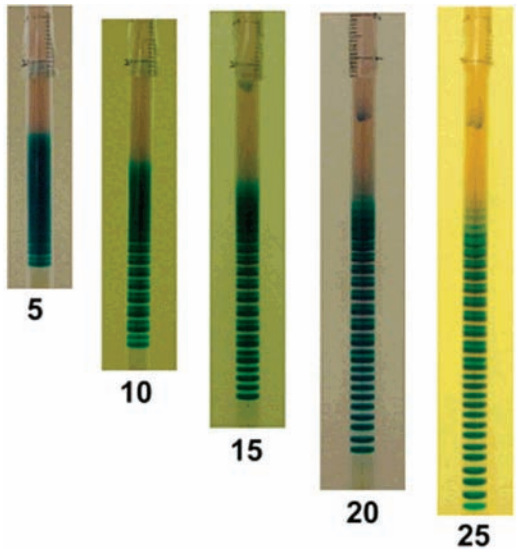

Figure 6. Time sequence of the propagating Liesegang pattern in experiment III: $[Co^{2+}]_0 = 0.175$ M, $[Ni^{2+}]_0 = 0.175$ M ($\delta = 0$); $[NH_4OH]_0 = 13.37$ M. The bands appear as close doublets which become well-resolved as they form further away from the interface.

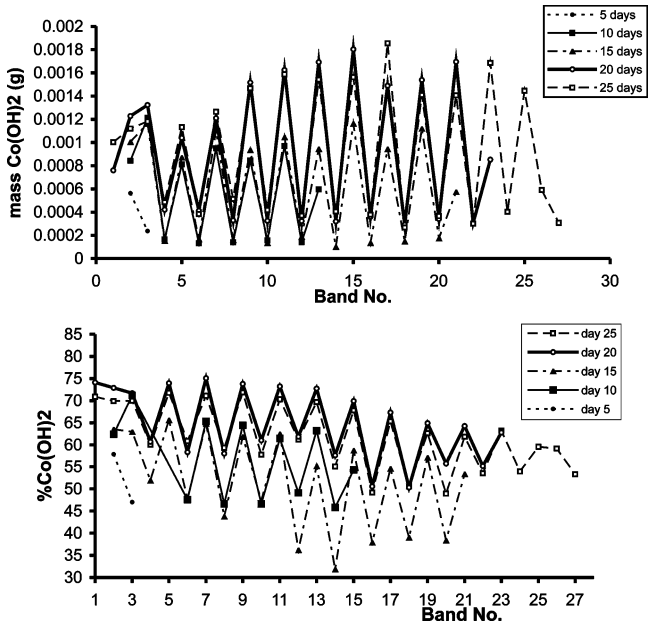

Figure 7. Distinct oscillations in the mass of $Co(OH)_2$ and $Co(OH)_2$ mass percent composition over the successive bands of the pattern in experiment III, shown in Figure 6.

different composition. The darker band indicates a larger mass and a higher percentage of $Co(OH)_2$ at a given time, whereas the less intense band has a smaller mass and a higher percentage of $Ni(OH)_2$.

The overall trend of the spatial distribution of the percent $Co(OH)_2$ composition cannot be directly determined when such marked oscillations exist. For this reason, the masses of the two precipitates in the pair of split bands (a doublet) were summed

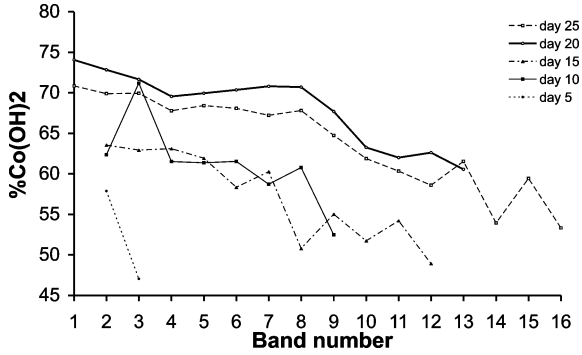

Figure 8. Regularization of the oscillations in Figure 7, as the doublets are combined each into one band, and the percent composition in $Co(OH)_2$ recalculated in the entire combined band. The oscillations are smoothened, reproducing the overall decreasing trend of random nature obtained in experiments I and II (Figures 4 and 5c).

up, and the total percentage composition by mass of $Co(OH)_2$ was recalculated and plotted versus band number. The overall trend, shown in Figure 8, now resembles that in the preceding two systems. Therefore, a consistent behavior of an overall decreasing trend in the $Co(OH)_2$ percent mass composition with band number is observed for the three experiments. Recall that, across the three sets, $[Co^{2+}]_0$ and $[Ni^{2+}]_0$ vary from widely distant to equal concentrations, with $[Co^{2+}]_0 \geq [Ni^{2+}]_0$.

3.3. Comparison of the Three Experiments. In this section, the spatial distributions of the patterns in experiments I−III at a given, fixed time are compared. This is done by first obtaining the statistical best-fit linear regression plots of the percentage of $Co(OH)_2$ versus band number, then calculating the slopes of the obtained straight lines, and finally comparing these slopes for the three different patterns at the same fixed time. All three sets show an overall decreasing trend in the percent composition of cobalt hydroxide with increasing band number. The statistical program SPSS[29] was used to test such decreasing trends by applying Pearson's correlation. It was found that the variables (percent $Co(OH)_2$ composition versus band number) are negatively correlated, with the correlations being significant at the 0.01 level in the best case and the 0.05 level in the worst case, for the three sets of experimental data and at all times. This decrease, however, becomes smoother as the concentrations of Co^{2+} and Ni^{2+} become more widely distant, since the plot of the percentage of $Co(OH)_2$ versus band number at the same time becomes distinctly less steep. Therefore, the overall trend is a general decrease in the mass percent of $Co(OH)_2$ with band number, in all three experiments. This implication is quantified by comparing the slopes of the lines for each of the three experiments at a fixed time. The results are shown in Table 2.

As the concentration difference δ decreases at fixed time, the variation of percent cobalt hydroxide with band number becomes more pronounced (the slope of the plot becomes more negative). There is a steeper decrease in $Co(OH)_2$ composition with new band formation at lower δ values. We illustrate this important result by selecting a fixed time ($t = 25$ days) and displaying a plot of percent $Co(OH)_2$ versus band number on the same graph for the three experiments. Such a comparison

TABLE 2: Slopes of Straight Lines Obtained from Linear Regression Analysis of the Percent $Co(OH)_2$ versus Band Number Plots, at Five Times, for the Three Separate Experiments I−III

					slopes at time shown (days)				
expt no.	$[Co^{2+}]_0$ (M)	$[Ni^{2+}]_0$ (M)	δ	ρ	5	10	15	20	25
I	0.250	0.100	0.15	2.5	0.267	−0.418	−0.3271	−0.461	−0.081
II	0.200	0.150	0.05	1.33	−0.194	−0.275	−0.532	−1.100	−0.141
III	0.175	0.175	0.00	1.00	−10.83	−1.542	−1.487	−1.065	−1.114

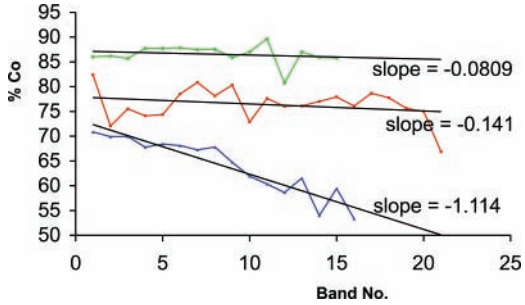

Figure 9. Variation of percent $Co(OH)_2$ with band number at $t = 25$ days for experiments I ($\delta = 0.150$), II ($\delta = 0.050$), and III ($\delta = 0$). As δ decreases, the trend becomes steeper with more negative slopes of the straight lines. The calculated slopes are shown in the figure and are the same as those in Table 2 at 25 days.

TABLE 3: Time Variation of the Average Mass Percent of $Co(OH)_2$ for Experiments I−III, Calculated over All the Bands[a]

	av % $Co(OH)_2$		
time (days)	expt I ($\delta = 0.15$ M)	expt II ($\delta = 0.05$ M)	expt III ($\delta = 0$)
5	74.9	64.4	52.5
10	90.8	80.7	61.3
15	93.2	83.8	57.4
20	90.6	85.7	68.2
25	86.6	75.2	64.0

[a] In each experiment, the average passes through a maximum. The corresponding plots are shown in Figure 10.

is highlighted in Figure 9. Days 10 and 20 present exceptions where the trend is slightly broken. Day 5 is no break of the trend (Table 2), as we go from positive to negative to more negative. Decreasing the concentration of cobalt in the gel relative to nickel (decreasing δ) generally decreases its percentage composition within the bands. This explains why the higher δ curves lie above the lower δ ones. At all times, however, the overall trend is a decrease in the percent composition of $Co(OH)_2$ with band number for the three sets. We further note that increasing the concentration of nickel and decreasing that of cobalt in the gel in a way to bring them closer to each other (smaller δ) results in a sharper decrease with band number at a fixed time. Thus, we see that as $[Ni^{2+}]_0$ is increased at the expense of $[Co^{2+}]_0$, not only is dissolution of $Ni(OH)_2$ more pronounced but also the dissolution event becomes more competitive between the top and the bottom of the tube, leading to the slopes being more negative than at higher δ (see notably Figure 9).

3.4. Time Variation of Percentage Composition of $Co(OH)_2$. The time evolution of composition is studied by computing the average percent composition in mass of $Co(OH)_2$ over all the strata and plotting it versus time. Instead of monitoring the time variation of the composition of each individual band, we assume that the average composition over all the bands in a given pattern and its time variation are representative of the entire chemical dynamics. Initially, the average percentage of $Co(OH)_2$ increases with time, for a given set of initial concentrations. This trend is reversed, however, as we go beyond a certain time. The time variations of the average mass percent of $Co(OH)_2$ for the three experiments, calculated over all the bands, are recorded in Table 3 and plotted in Figure 10.

In each experiment, the aforementioned average passes through a maximum, as indicated by the trend lines drawn by interpolation in Figure 10. This switch in the trend as the time

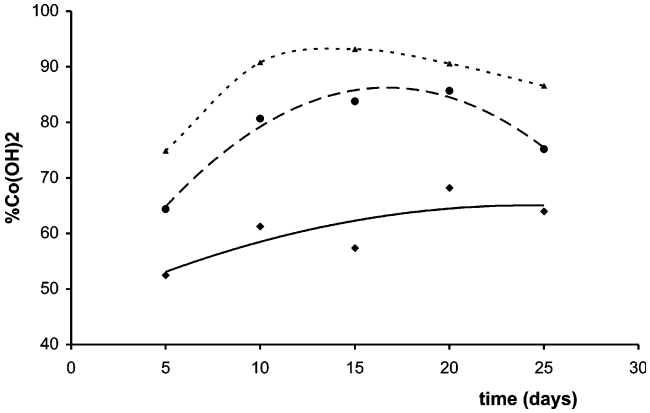

Figure 10. Time evolution of the mass percent composition in $Co(OH)_2$, calculated over all the strata: (◆) $\delta = 0$; (●) $\delta = 0.05$; (▲) $\delta = 0.15$. The composition does not show a monotonic increase as one would expect. Over this time range (5−25 days, at 5 day intervals), it exhibits an increase followed by a decrease. Note that as $[Ni^{2+}]_0$ decreases (δ increases), the percent $Co(OH)_2$ is higher at any time.

increases is very interesting and reveals a competition scenario between precipitation and dissolution as the time advances. As the NH_4OH concentration starts to decrease after this maximum (diffusion profile smoothens) and becomes insufficient for the effective dissolution of cobalt hydroxide, and most notably nickel hydroxide, the precipitation becomes dominant. A dominant precipitation at large times favors $Ni(OH)_2$ being regained at the expense of $Co(OH)_2$, which clearly explains the switch observed in Figure 10. Furthermore, different maxima are obtained at different times for each of the three sets (experiments I−III). The interpolation lines reveal maxima in the percentage of $Co(OH)_2$ at days 13 and 17 with values of 93% and 86% for experiments I and II, respectively. The maximum in the trend line of experiment III is not clear but definitely occurs at a later time (the last point is 64% at day 25). Thus, the maximum occurs earlier in time as $[Ni^{2+}]_0$ decreases (δ increases). It is delayed as we go from experiment I to II to III. This is expected on the basis of the initial concentrations of both cations in the gel. As $[Ni^{2+}]_0$ is decreased (experiment III to II to I), its precipitation becomes favored over its dissolution, thus causing a switch in the increase in $Ni(OH)_2$ to occur earlier in time (earliest in experiment I at 13 days, when $[Ni^{2+}]_0$ is least).

4. Theoretical Modeling

We now attempt to simulate the dynamics of the above system by setting up the evolution equations describing the diffusion of all aqueous species involved, coupled to the kinetics of precipitation and redissolution. After simplifying the reaction scheme given by eqs 1−4, we write the reaction−diffusion equations in conformity with the model of Polezhaev and Müller,[30] wherein the precipitate particles evolve through three main stages: birth of nuclei, transition of nuclei into particles, and finally growth of particles toward an equilibrium state. Each of the aforementioned stages is governed by a typical, characteristic threshold of the aqueous monomer $Co(OH)_2(aq)$ or $Ni(OH)_2(aq)$ with concentration c. The model, initially developed for a simple salt system of the type AB,[30] is adapted here for the full-fledged scenario involving the two precipitates $Co(OH)_2$ and $Ni(OH)_2$ (eqs 1−4), with the exact stoichiometry. This latter treatment was carried out by Al-Ghoul and Sultan[2] for the $Co(OH)_2$ system and was extended in a preliminary treatment to the two-precipitate study by Shreif et al.[1] Electrical effects were added to the model in ref 3.

4.1. Model and Evolution Equations. The scheme of eqs 1−4 is simplified to a kinetic model which captures the essence of the physicochemical processes involved. The representative chemical equations are

$$X + 2Y \xrightarrow{k_1} 2Z + A \tag{5}$$

$$A + 6Z \xrightarrow{k_1'} P \tag{6}$$

$$W + 2Y \xrightarrow{k_2} 2Z + B \tag{7}$$

$$B + 6Z \xrightarrow{k_2'} Q \tag{8}$$

where X ≡ Co^{2+}, W ≡ Ni^{2+}, Y ≡ NH_4OH, Z ≡ NH_4^+, A ≡ $Co(OH)_2$, B ≡ $Ni(OH)_2$, and P and Q are the products of the $Co(OH)_2$ and $Ni(OH)_2$ redissolution reactions, respectively. Let C_X, C_Y, C_Z, and C_W denote the concentrations of the species X, Y, Z, and W, respectively. Furthermore, we define C_A as the concentration of the dissolved salt $Co(OH)_2$(aq), and C_B that of $Ni(OH)_2$(aq), from which the precipitate nuclei will form and grow. We let $\tilde{\rho}_A$ and $\tilde{\rho}_B$ be the precipitate densities (of A and B) as nuclei and ρ_A and ρ_B the precipitate densities as particles. The kinetic evolution equations describing the dynamics of the aqueous species X, Y, W, Z, A(aq), and B(aq), along with the precipitate densities $\tilde{\rho}_A$, ρ_A, $\tilde{\rho}_B$, and ρ_B, are given by the following coupled nonlinear system of reaction−diffusion equations:

$$\frac{\partial \mathbf{C}}{\partial t} = \mathbf{D}\nabla^2\mathbf{C} + \mathbf{F} \tag{9}$$

where **C** denotes the vector of concentrations of the aforementioned species and is given by

$$\mathbf{C} = (C_X, C_Y, C_Z, C_W, \tilde{\rho}_A, \rho_A, \tilde{\rho}_B, \rho_B, C_A, C_B)^T \tag{10}$$

and **D** is a diagonal matrix whose elements are the corresponding diffusion coefficients of those species:

$$\mathbf{D} = \mathrm{diag}(D_X, D_Y, D_Z, D_W, 0, 0, 0, 0, D_A, D_B)$$

The nonlinear vector **F** is given by

$$\mathbf{F} = \begin{pmatrix} -k_1 C_X C_Y^2 \\ -2k_1 C_X C_Y^2 - 2k_2 C_W C_Y^2 \\ 2k_1 C_X C_Y^2 + 2k_2 C_W C_Y^2 - 6C_Z^6(k'_1\rho_A + k'_2\rho_B) \\ -k_2 C_W C_Y^2 \\ \upsilon_1(C_A) - [\upsilon_2(C_A) + \upsilon_3(C_A)]\tilde{\rho}_A \\ \upsilon_3(C_A)\tilde{\rho}_A + \upsilon_4(C_A)\rho_A - 6k'_1 C_Z^6 \rho_A \\ \upsilon_1(C_B) - [\upsilon_2(C_B) + \upsilon_3(C_B)]\tilde{\rho}_B \\ \upsilon_3(C_B)\tilde{\rho}_B + \upsilon_4(C_B)\rho_B - 6k'_2 C_Z^6 \rho_B \\ k_1 C_X C_Y^2 - \upsilon_1(C_A) + \upsilon_2(C_A)\tilde{\rho}_A - \upsilon_4(C_A)\rho_A + 6k'_1 C_Z^6 \rho_A \\ k_2 C_W C_Y^2 - \upsilon_1(C_B) + \upsilon_2(C_B)\tilde{\rho}_B - \upsilon_4(C_B)\rho_B + 6k'_2 C_Z^6 \rho_B \end{pmatrix} \tag{11}$$

The sixth-order kinetic rate law involving the complexation of ammonia with the metal ions, which appears in the kinetic equations (11), arises from a preequilibrium kinetic treatment of successive additions, each involving one ammonia molecule. The overall equilibrium constant of the five sucessive complex formation steps is

$$K_5 = \beta_1\beta_2\beta_3\beta_4\beta_5 = \frac{[M(NH_3)_5^{2+}]}{[M][NH_3]^5} \tag{12}$$

where the β_i values are the five successive formation constants and M is the metal ion (Co^{2+} or Ni^{2+}). The sixth step (addition of NH_3 to $M(NH_3)_5^{2+}$), with rate constant k_6, is rate-determining and has the rate law

$$\frac{d[M(NH_3)_6^{2+}]}{dt} = k_6[M(NH_3)_5^{2+}][NH_3] = k_6K_5[M][NH_3]^6 \tag{13}$$

yielding a rate law that is sixth order in ammonia, with the rate constant $k' = k_6K_5$. Note that this preequilibrium treatment is shown here for the free M^{2+} ion, for simplicity. The exact treatment should reflect the formation of the complex from the redissolution of the precipitate: i.e., starting from $M(OH)_2$ and the released ammonium ion NH_4^+. This redissolution is referred to in the literature as redissolution in the third electrolyte (i.e., NH_4Cl).[11,12] The complete set of equations is displayed in Appendix B. Note that ammonium ion was shown (by Shreif et al.[1]) to play a key role as an intermediate and govern the entire dynamics of the system. The NH_3/NH_4^+ equilibrium reaction is not considered here, in view of the large predominance of the precipitation and redissolution reactions and in conformity with other simplified models treating Liesegang dynamics with redissolution by complex formation.[16,17] The mass balance equations for Co and Ni over the entire spatial span of the tube are presented and discussed in Appendix A.

The equations (9) are supplemented with the appropriate initial conditions, no-flux boundary conditions, and criticality conditions for C_A and C_B, which are described in detail in ref 2. The rate function terms $\upsilon_1(C)$, $\upsilon_2(C)$, $\upsilon_3(C)$, and $\upsilon_4(C)$ and their dependence on the concentration of the dissolved monomers C_A and C_B are characterized by expressions involving the Heaviside step function, on the basis of the aforementioned criticality conditions. The equations in the set (9) are discretized using a second-order central finite difference scheme in space, and the resulting ordinary differential equations are then solved using an adaptive backward differencing scheme, due to the stiffness of the system. Throughout the reported computation, we used 400 spatial grid points with a grid size of 0.25 and a relative tolerance of 10^{-6}. Lowering the grid size to 0.01, using a fourth-order central finite difference scheme for the Laplacian, or increasing the spatial grid to 800 did not change the results quantitatively. A complete description of the problem is found in refs 2 and 30.

4.2. Results. The equations (9) are solved numerically using a finite difference scheme in space and a backward difference formula in time.

Figure 11 shows the spatial distribution of the density of precipitates A and B, ρ_A and ρ_B, respectively, along with its time evolution. We see that the $Co(OH)_2$ bands (blue) and the $Ni(OH)_2$ bands (red) overlap, as we obtained in the experiments. The pattern evolves with time as we go from frame **a** to frame **c**. The mass of $Co(OH)_2$ and $Ni(OH)_2$ in a given band was determined by integration under the density peak between its edges, in a domain where a blue band and a red band overlap. The percent composition was then calculated for each precipitate by summing the two masses and calculating the ratio of the mass of the desired salt over the total mass. The computation was then repeated for every stratum in the skeleton at a fixed chosen time. A plot of percent $Co(OH)_2$ versus band number at a fixed time is depicted in Figure 12, for three different sets of

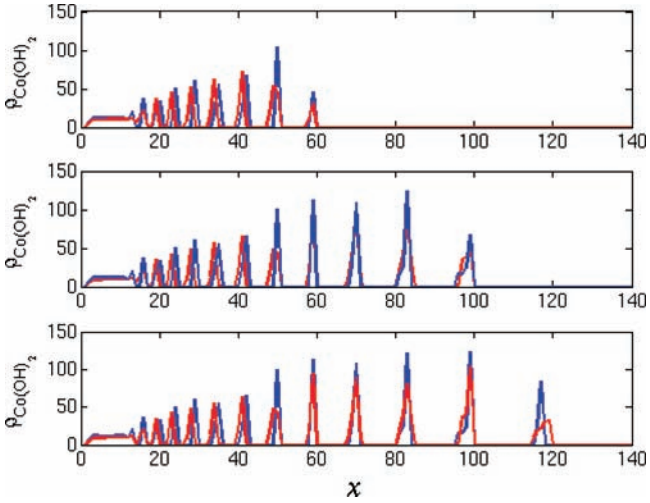

Figure 11. Bands of $Co(OH)_2$ (blue) and $Ni(OH)_2$ (red) obtained from the solution of eqs 9 and 11, with pattern evolution at three different times. The bands essentially overlap, enabling a calculation of mass percentage for each precipitate by integration. Model parameters: $X_0(Co^{2+}) = 10$; $Y_0 = 250$; $W_0(Ni^{2+}) = 10$; $k_1 = 0.0001$; $k'_1 = 0.01$; $k_2 = 0.0001$; $k'_2 = 0.1$; $D_X = D_Y = D_W = 1 \times 10^{-5}$; $D_Z = 1 \times 10^{-4}$; $D_A = D_B = 1 \times 10^{-5}$. For both C_A and C_B, the critical parameters were $c_1 = 2.1$, $c_2 = 2$, and $c_3 = 3$.

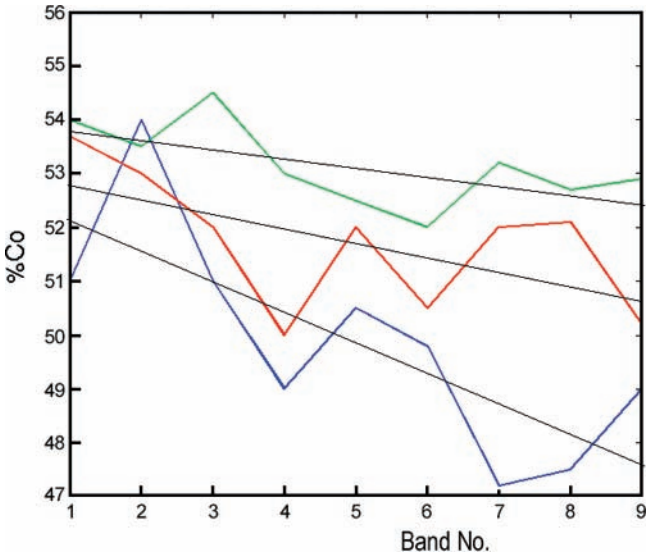

Figure 12. Percent $Co(OH)_2$ versus band number for three runs with different initial concentrations of Co^{2+} and Ni^{2+}: (green curve) $[Co^{2+}]_0 = 20$, $[Ni^{2+}]_0 = 5$ ($\delta = 15$), slope -0.0017; (red curve) $[Co^{2+}]_0 = 15$, $[Ni^{2+}]_0 = 7$ ($\delta = 8$), slope -0.0027; (blue curve) $[Co^{2+}]_0 = 10$, $[Ni^{2+}]_0 = 10$ ($\delta = 0$), slope -0.0057. As δ decreases with an increase in $[Ni^{2+}]_0$, the plots become steeper, exactly reproducing the experimental results of Figure 9.

initial concentrations. The first striking result is the random variation of percent composition with band number. The nonlinear dynamics of diffusion, precipitation, and redissolution in such a complex multiple-species system seems to be governed by an oscillatory regime, characterizing the competition between precipitation and redissolution. The random nature of the variation probably originates from the depletion following the formation of a certain band, wherein the new buildup of the concentration profiles for the species in solution follows a different distribution of a random nature after each band formation. This new set of conditions after every band formation is caused by the nonequilibrium state of the band evolution, which is maintained as the system is depleted and waiting for replenishment by diffusion. The most interesting result in the

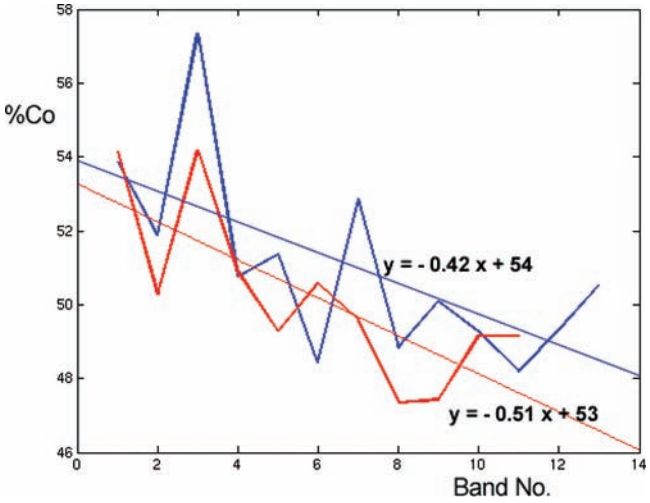

Figure 13. Percent $Co(OH)_2$ versus band number for two runs with different initial concentrations of NH_4OH: (red curve) $[Co^{2+}]_0 = [Ni^{2+}]_0 = 10$, $[NH_4OH]_0 = Y_0 = 200$; (blue curve) $[Co^{2+}]_0 = [Ni^{2+}]_0 = 10$, $[NH_4OH]_0 = Y_0 = 250$. The plot with lower NH_4OH initial concentration (red) is steeper, exhibiting a more negative slope.

present study is that those random composition variations exactly reproduce the erratic behavior obtained experimentally (compare notably Figure 12 with Figure 9). Thus, those oscillations appear to be inherent in the system dynamics and are not the mere result of random errors in the analysis. Over a large set of trials of refined quality, it was impossible to get a monotonic and smooth trend. The overall trend over a given pattern of 1D strata, however (fixed time), is a general decrease in the percent mass of $Co(OH)_2$. This is revealed by the negative slope of the best-fit straight line plotted for each of the three runs in Figure 12, which also reproduces our experimental results (see notably Figure 9). The overall decrease is no doubt caused by the fact that, near the gel−solution junction, redissolution is more pronounced (higher NH_4^+ concentration). The three curves of Figure 12 correspond to three different initial experimental conditions. As we go from plot a (green) to b (red) to c (blue), the concentration of Ni^{2+} is increased (smaller value of the concentration difference δ) and the dynamics yields more negative slopes of the best-fit straight lines, in complete harmony with our experimental findings (please refer to Table 2 as well as Figures 4, 5c, and essentially 9).

The same random oscillations and transition toward a more rapid decrease in percent $Co(OH)_2$ (more negative slope of best fit) are seen if we *decrease* the concentration of the outer electrolyte ($Y_0 \equiv [NH_4OH]_0$). This is illustrated in Figure 13. Here $[Co^{2+}]_0 = [Ni^{2+}]_0 = 10$, while $[NH_4OH]_0$ is varied. The trend of decreasing percent $Co(OH)_2$ with increasing band number is maintained for the same argument, whereby the percent $Ni(OH)_2$ is larger far away from the junction because of the weakened effect of redissolution. The higher Y_0 value is seen to ease and tame the effect of differentiated composition in space (between the top and the bottom of the tube). Although redissolution is enhanced, precipitation at high Y_0 seems to be the dominant factor here, since both $Co(OH)_2$ and $Ni(OH)_2$ precipitate to a large extent, even at large distances from the interface. The spatially differentiated composition is thus more enhanced (more negative slope) at lower $[NH_4OH]_0$ (Y_0). This is supported by the faster kinetics of precipitation for $Co(OH)_2$, as argued before in section 3.1.2 (experiment II, paragraph before the last).

Finally, the time evolution is conjectured in Figures 14 and 15. Figure 14 shows the composition distribution over the band

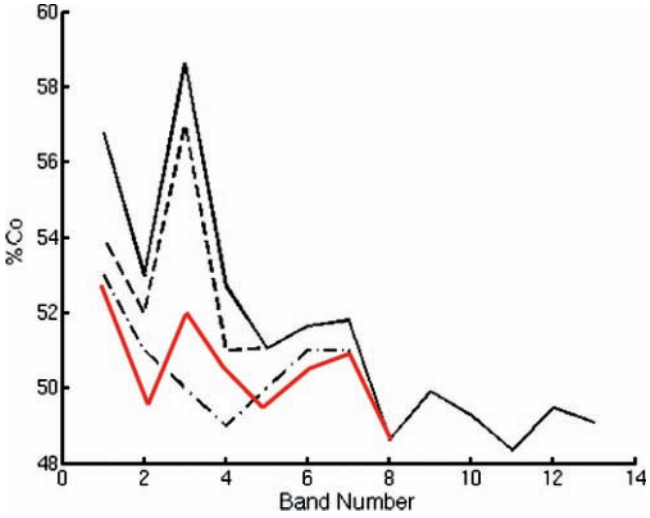

Figure 14. Perecent $Co(OH)_2$ versus band number at four different times: (red curve) $t_1 = 5 \times 10^5$; (solid black curve) $t_2 = 10 \times 10^5$; (dashed curve) $t_3 = 15 \times 10^5$; (dotted-dashed curve) $t_4 = 20 \times 10^5$. Other conditions: $[Co^{2+}]_0 = [Ni^{2+}]_0 = 9$; $[NH_4OH]_0 = Y_0 = 200$.

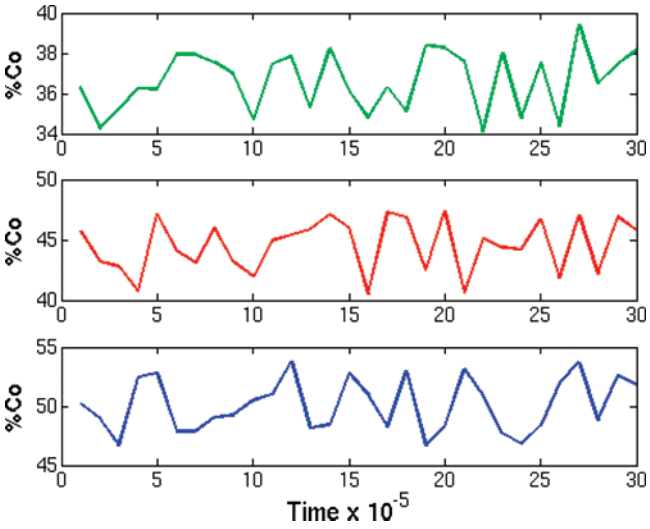

Figure 15. Time variation of the mass percent of $Co(OH)_2$ *over the whole pattern*. The three curves correspond to three different sets of Co^{2+} and Ni^{2+} initial concentrations. The time dependence is seen to display random oscillations, of which the trend in Figure 10 appears to be only a small portion: (blue curve) $[Co^{2+}]_0 = [Ni^{2+}]_0 = 10$; (red curve) $[Co^{2+}]_0 = 10$, $[Ni^{2+}]_0 = 15$; (green curve) $[Co^{2+}]_0 = 10$, $[Ni^{2+}]_0 = 20$. For all experiments $[NH_4OH]_0 = Y_0 = 200$.

strata in the same experiment, at four different times. The random oscillations with band number are clearly maintained (a crucial dynamic property of this complex system), As for the time advancement, we start with low percent $Co(OH)_2$ overall (red curve), which then jumps to high values (solid black) and degrades back to lower percentages (dashed line followed by dash-dotted line). This exactly captures the features illustrated by the location of the curves at different times in Figures 4 and 5b,c, notably the time dependence of the total percent $Co(OH)_2$ exhibited in Figure 10. The dynamics of the present system reveals an even higher complexity when the analogue of Figure 10 is conjectured. We compute the time dependence of the total percent Co composition over all the bands for three different sets of initial concentrations. The results are depicted in Figure 15. Because the calculations could be performed for longer times, and over more frequent time intervals than in the experiments, we see that the total percent Co composition exhibits interesting temporal oscillations of random nature. It thus seems that the maxima observed in Figure 10 represent a behavior of a more general random nature as time advances and when more time intervals are monitored. The plots of Figure 10 thus appear to actually reproduce small fragments of the more comprehensive plots of Figure 15.

The present study has unraveled a good deal of information about the dynamics of multicomponent Liesegang systems involving precipitate redissolution. The complexity of the dynamics emerges from a twofold variant from a classical Liesegang patterning system: (1) chemical complex formation which triggers redissolution and thus adds to the diversity of the chemical processes; (2) the presence of two precipitates, thus yielding a count of two precipitation and two redissolution reactions. This multitude of processes and chemical species involved yields the complex system of nonlinear equations in the model given by eqs 9−11. In a recent study,[31] a shift in the experiment to special conditions wherein $[Co^{2+}]_0 = 0.250$ M and $[Ni^{2+}]_0 = 0.200$ M yielded an interesting pattern with exotic morphological characteristics. A further elucidation of this complex dynamic system includes the determination of the profiles of all the aqueous species involved along with their time evolution, as well as a systematic characterization of the random oscillations from the viewpoint of a Chaos analysis. This is the subject of current and future investigations.

Acknowledgment. This work was supported by the University Research Board (URB) of the American University of Beirut. We thank the director and staff of the Central Research Science Lab (CRSL) at the American University of Beirut (AUB) for all of the atomic absorption measurements.

Appendix A: Mass Balance for Co and Ni

The total cobalt concentration in the system is at any time equal to $[Co^{2+}]_0$, the concentration of cobalt ions initially present in the gel (prepared as described in section 2). This cobalt is transformed into the following species throughout the tube: $Co(OH)_2(s)$, $Co(NH_3)_6^{2+}(aq)$, and $Co(OH)_2(aq)$. The last species represents the dissolved salt particles, which are known to exist even between the bands. Therefore, the mass balance of cobalt in the total volume of the gel in the tube can be written as

$$[Co^{2+}]_0 = [Co^{2+}] + [Co(NH_3)_6^{2+}(aq)] + [Co(OH)_2(aq)] + \frac{m_{Co(OH)_2}(s)}{M_{Co(OH)_2} \times V} \quad (14)$$

where V is the total volume of the gel, $M_{Co(OH)_2}$ is the molar mass of cobalt hydroxide, and $[Co^{2+}]$ is the concentration of free (unreacted) cobalt ions in the gel. In the reported experiments, the masses of cobalt hydroxide, $m_{Co(OH)_2(s)}$, and nickel hydroxide, $m_{Ni(OH)_2(s)}$, and the subsequent mass percents in each precipitate were measured using atomic absorption, as described at the end of section 2. Though embedded in a gel, the Co element in the analyzed portion was assumed to be contained solely in the precipitate; Co^{2+}, $Co(NH_3)_6^{2+}(aq)$, and $Co(OH)_2(aq)$ within the band zone were considered to be negligible. The validity of the mass balance can only be tested if all the remaining terms $[Co^{2+}]$, $[Co(NH_3)_6^{2+}(aq)]$, and $[Co(OH)_2(aq)]$ in *all* the bands and gel portions are measured. This interesting and minute experimental endeavor constitutes a fundamentally tedious task and was not attempted here.

Theoretically, the validity of mass balance can be estimated by computation using a similar expression. Using the same notation as in section 4.1, $[Co^{2+}] = X_0 - \bar{X}(t)$, where $\bar{X}(t)$ is

the average cobalt ion concentration over a tube of length L and can be written as $\bar{X}(t) = \int_0^L X(x,t)\,dx$. $[Co(OH)_2(aq)]$ is represented by $\bar{C}_A(t) = \int_0^L C_A(x,t)\,dx$, and the mass of the solid cobalt hydroxide $m_{Co(OH)_2(s)}$ is computed using the density of large particles $\bar{\rho}_A(t) = \int_0^L \rho_A(x,t)\,dx$. The complex concentration $[Co(NH_3)_6^{2+}(aq)]$ is considered as a sink product (P), and for simplicity, it was not taken into consideration in the model. The mass balance in this case can be written as

$$[Co^{2+}]_0 = X_0 - \bar{X}(t) + \bar{C}_A(t) + \bar{\rho}_A(t) + P$$

Here also, the mass balance cannot be rigorously checked, because we do not have information on the species P. This issue will be addressed in future work.

Appendix B: Redissolution of $M(OH)_2$ and Preequilibrium Kinetics for the Successive Complex Formation Reactions

The successive complex formation reactions are

$$M(OH)_2 + NH_4^+ \rightleftharpoons MNH_3(OH)^+ + H_2O$$

$$MNH_3(OH)^+ + NH_4^+ \rightleftharpoons M(NH_3)_2^{2+} + H_2O$$

$$M(NH_3)_2^{2+} + NH_4^+ + OH^- \rightleftharpoons M(NH_3)_3^{2+} + H_2O$$

$$M(NH_3)_3^{2+} + NH_4^+ + OH^- \rightleftharpoons M(NH_3)_4^{2+} + H_2O$$

$$M(NH_3)_4^{2+} + NH_4^+ + OH^- \rightleftharpoons M(NH_3)_5^{2+} + H_2O \quad (15)$$

Net preequilibrium reaction:

$$M(OH)_2 + 5NH_4^+ + 3OH^- \overset{K_5}{\rightleftharpoons} M(NH_3)_5^{2+} + 3H_2O$$

Rate-determining step:

$$M(NH_3)_5^{2+} + NH_4^+ + OH^- \xrightarrow{k_6} M(NH_3)_6^{2+} + H_2O$$

Thus:

$$\frac{d[M(NH_3)_6^{2+}]}{dt} = k_6[M(NH_3)_5^{2+}][NH_4^+][OH^-] = k_6K_5[M(OH)_2][OH^-]^4[NH_4^+]^6$$

which is equivalent to the rate law of a single-step redissolution reaction (eqs 2 and 4) with $k' = k_6K_5$, as obtained in eq 13 for the free M^{2+} ion. In the theoretical modeling, this equation is simplified to eqs 6 and 8, wherein $[M(OH)_2]$ is treated as a constant: namely, the density of the precipitate (ρ_A or ρ_B). Note that the model is simplified by taking $[OH^-]$ as a constant (such as assuming a constant pH), and hence $k' = k_6K_5[OH^-]^4$ is a pseudo-sixth-order rate constant. Thus, the sixth-order kinetic rate law (in the intermediate NH_4^+), which appears in eq 11, is justified.

References and Notes

(1) Shrief, Z.; Al-Ghoul, M.; Sultan, R. *Chem. Phys. Chem.* **2002**, *3*, 592.
(2) Al-Ghoul, M.; Sultan, R. *J. Phys. Chem. A* **2001**, *105*, 8053−8058.
(3) Al-Ghoul, M.; Sultan, R. *J. Phys. Chem. A* **2003**, *107*, 1095−1101.
(4) Ball, P. *The Self-Made Tapestry: Pattern Formation in Nature*; Oxford University Press: Oxford, U.K., 1999.
(5) Liesegang, R. E. *Chem. Fernwirk. Lieseg. Photograph. Arch.* **1896**, 37, 305, 331.
(6) Henisch, H. *Crystals in Gels and Liesegang Rings*; Cambridge University Press: Cambridge, U.K., 1988.
(7) Stern, K. H. *Chem. Rev.* **1954**, *54*, 79.
(8) Kapral, R.; Showalter, K. *Chemical Waves and Patterns*; Kluwer Academic: Dordrecht, The Netherlands, 1995.
(9) Shreif, Z.; Mandalian, L.; Abi-Haydar, A.; Sultan, R. *Phys. Chem. Chem. Phys.* **2004**, *6*, 3461.
(10) Nasreddine, V.; Sultan, R. *J. Phys. Chem. A* **1999**, *103*, 2934.
(11) Lloyd, F. E.; Moravek, V. *Plant Physiol.* **1928**, *3*, 101.
(12) Ostwald, W. *Kolloid-Z.* **1925**, *36*, 380.
(13) Das, I.; Pushkarna, A.; Argawal, N. R. *J. Phys. Chem.* **1987**, *91*, 747.
(14) Zrĭnyi, M.; Gálfi, L.; Smidróczki, É.; Rácz, Z.; Horkay, F. *J. Phys. Chem.* **1991**, *95*, 1618.
(15) Sultan, R.; Panjarian, Sh. *Physica D* **2001**, *157*, 241.
(16) Lagzi, I. *J. Phys. Chem. B* **2003**, *107*(49), 13750−13753.
(17) Izsák, F.; Lagzi, I. *J. Phys. Chem. A* **2005**, *109*(5), 730−733.
(18) Schaeffer, C. D.; Strausser, C. A.; Thomsen, M. W.; Yoder, C. H. *Data for General, Organic and Physical Chemistry*; available from http://wulfenite.fandm.edu/Data%20/Data.html; accessed in 2003.
(19) Meites, L. *Handbook of Analytical Chemistry*, 1st ed.; McGraw-Hill, New York, 1963.
(20) Attieh, M.; Al-Kassem, N.; Sultan, R. *J. Chem. Soc., Faraday Trans.* **1998**, *194*, 2187−2194.
(21) Sultan, R.; Al-Kassem, N.; Sultan, A. A-H.; Salem, N. *Phys. Chem. Chem. Phys.* **2000**, *2*, 3155−3162.
(22) Mandalian, L.; Fahs, M.; Al-Ghoul, M.; Sultan, R. *J. Phys. Chem. B* **2004**, *108*, 1507−1514.
(23) Msharrafieh, M.; Sultan, R. *Chem. Phys. Chem.* **2005**, *6*(12), 2647−2653.
(24) Sultan, R.; Sadek, S. *J. Phys. Chem.* **1996**, *100*, 16912.
(25) Droz, M.; Magnin, J.; Zrinyi, M. *J. Chem. Phys.* **1999**, *110*, 9618−9622.
(26) Jablczynski, C. K. *Bull. Soc. Chim. Fr.* **1923**, *11*, 1592.
(27) Antal, T.; Droz, M.; Magnin, J.; Rácz, Z.; Zrinyi, M. *J. Chem. Phys.* **1998**, *109*, 9479.
(28) Müller, S. C.; Kai, S.; Ross, J. *J. Phys. Chem.* **1982**, *86*, 4078.
(29) SPSS Advanced ModelsTM 12.0; SPSS Inc., http://www.spss.com; accessed on 2004.
(30) Polezhaev, A. A.; Müller, S. C. *Chaos* **1994**, *4*, 631−636.
(31) Msharrafieh, M.; Sultan, R. *Chem. Phys. Lett.* **2006**, *421*(1−3), 221−226.